J Mater Sci (2006) 41:7944–7953
DOI 10.1007/s10853-006-0863-4

Effects of calcium nitride and calcium carbonate gasifying agents on the porosity of Ni_3Ti–TiC composites produced by combustion synthesis

Douglas E. Burkes · Jack Milwid · Guglielmo Gottoli · John J. Moore

Received: 5 July 2005 / Accepted: 15 November 2005 / Published online: 21 September 2006

Abstract Combustion synthesis or Self-propagating High Temperature Synthesis (SHS) has been used to produce highly porous materials intended for biomedical applications. Two novel gasifying agents, calcium nitride and calcium carbonate, were employed to increase product porosity and pore size during the combustion synthesis reaction for two SHS chemical compositions. A greater increase in apparent porosity of the products was gained using calcium carbonate compared with calcium nitride. Conversely, a greater increase in the number of pores falling within a 101–500 μm range was gained using calcium nitride compared with calcium carbonate. A greater increase in product porosity and pore sizes was observed for the TiC-50 wt% Ni_3Ti than the TiC-30 wt% Ni_3Ti with both gasifying agents.

Introduction

Combustion synthesis, or Self-propagating High-temperature Synthesis (SHS), is an alternative technique for producing advanced ceramics, ceramic composites and intermetallic compounds and is dependent upon a highly exothermic chemical reaction becoming self-sustaining after a short energy pulse is applied to initiate the reaction [1]. Porosity in the synthesized product is typical by (1) initial relative 'green' density of the powder compact, (2) change in volume between the reactants and products, (3) volatilization of impurities at high temperatures during the process and (4) electron migration [2]. There are a number of factors that contribute to porosity, pore size and pore distribution of the synthesized product. Examples of these factors are the initial porosity of the starting sample, capillary effects, volume exchange between initial reactants and final products, reactant particle size and viscosity of liquid generated at the combustion front [3–7].

Highly porous materials (e.g. >60%) can be produced using combustion synthesis when the reactants and products remain in a solid state, and is largely the result of initial porosity in the unreacted powder compact. Gravity enhanced densification results if the combustion temperature exceeds the melting temperature of one or more of the reactants or products [8]. The molten reactants and/or product flow due to capillary effects and gravity, especially if there is significant difference in the densities of the molten and solid species resulting in densification of the sample, i.e. voids are filled with molten species. A gasifying agent can be introduced into the reaction front to overcome naturally occurring densification for such systems. For the gasifying agent to be effective in increasing product porosity, the liquid viscosity generated in the combustion wave should possess an optimum level of resistance to the transport of the gas through the liquid

This manuscript has not been published elsewhere and has not been submitted simultaneously for publication elsewhere. Part 2 of a two series document.

D. E. Burkes (✉) · J. Milwid · G. Gottoli · J. J. Moore
Metallurgical and Materials Engineering Department, Colorado School of Mines, 1500 Illinois Street, Golden, CO 80401-1887, USA
e-mail: dburkes@mines.edu

D. E. Burkes · G. Gottoli · J. J. Moore
Institute for Space Resources (ISR), Colorado School of Mines, Golden, CO 80401, USA

phase. If the viscosity is too high, the gas encounters an increased level of resistance and becomes trapped in the liquid during solidification. This results in undesired ''blow holes'', or extremely large and disorganized pores, in the product. Conversely, the gas encounters a decreased level of resistance and flows easily through the liquid if the viscosity is too low, usually resulting in little to no increase in product porosity. There is an optimum amount of liquid that should be generated at the reaction front to effectively increase and engineer product porosity. A high amount of liquid generated at the reaction front results in enhanced product densification, whereas a lesser amount of liquid will not entrap the flowing gas [9].

In some cases, significant gas evolution occurs during combustion synthesis due to out gassing of highly volatile impurities and adsorbed gases contained in the reactant powder, i.e. a mixture of titanium and carbon black (hygroscopic) [2, 10]. In other cases, novel gasifying agents are purposely added to the reactant mixture [9, 11]. Ideal gasifying agents posses a decomposition temperature around the combustion temperature of the reaction, thereby releasing gas(es) into the viscous reaction front to aid in creation of pores. There is little to no increase in product porosity if the gas is generated ahead of the reaction front due to considerable differences in the decomposition and combustion temperatures. The selected gasifying agent should not significantly interfere with or retard the combustion synthesis reaction as decomposition is typically an endothermic process, i.e. heat generated from the exothermic combustion synthesis reaction should far exceed the heat required to decompose the gasifying agent. The reaction could quench prior to reaching full conversion in cases where the gasifying agent acts as a significant diluent or heat sink. The reaction system must propagate with a relatively high burning velocity (e.g. stable, planar combustion wave) to minimize heat loss effects from the reaction front [9].

Porous combustion synthesis materials have shown promise as medical devices ranging from dental implants to bone and joint replacement implants, as well as additional applications such as heat exchangers, catalyst support systems, microfilters and ultra-light weight high strength materials [12–14]. Porosity of an implant is important when attempting to facilitate bone ingrowth and fixation into the implant. The minimum pore size for which bone growth can occur into biocompatible implants is 75 μm in diameter, the size required to accommodate an osteon [15]. However, the optimum pore size range observed in clinical practice ranges from 100 to 350 μm [16]. Typically, a material intended for a large bone replacement application requires porosity in the range of 40 to 60% [17], but this range is dependent upon the anatomical location of the implant. The porosity requirement is a large reason why most ceramics are not ideal for bone replacement applications. Materials produced using combustion synthesis have a high volume (~85–95%) of interconnected (open) pores that provide space for vascular tissue required for continued mineralized bone growth [18, 19]. Surface texturing of implants increases adsorption and proliferation of cells in vitro and in vivo, giving rise to the importance of surface morphology to curb implant rejection [20–23].

Experimental materials and methods

Two chemical compositions within the Ni_3Ti–TiC system were explored designated as TiC-30 wt% Ni_3Ti and TiC-50 wt% Ni_3Ti (nominal percentages). The chemical compositions were combined with a varying amount of calcium nitride (Ca_3N_2) or calcium carbonate ($CaCO_3$) gasifying agent to increase product porosity and pore size. The SHS equations used to generate the chemical compositions are presented in Equations 1 and 2.

$$x\mathrm{Ni}+(0.33x+y+2z)\mathrm{Ti}+y\mathrm{C}+z\mathrm{Ca_3N_2} = 0.33x\mathrm{Ni_3Ti}+y\mathrm{TiC}+2z\mathrm{TiN}+3z\mathrm{Ca(g)} \quad (1)$$

$$x\mathrm{Ni}+(0.33x+y)\mathrm{Ti}+y\mathrm{C}+z\mathrm{CaCO_3} = 0.33x\mathrm{Ni_3Ti}+y\mathrm{TiC}+z\mathrm{CaO}+z\mathrm{CO_2(g)} \quad (2)$$

Chemical compositions were prepared maintaining the amount of Ni_3Ti intermetallic present in the synthesized product and the amount of gas produced from the gasifying agent. The refractory phase and decomposition product varied for differing amounts and type of gasifying agent. Three molar amounts of each gasifying agent were investigated in addition to samples reacted with no gasifying agent for the TiC-30 wt% Ni_3Ti and TiC-50 wt% Ni_3Ti. Varying molar amounts of Ca_3N_2 and $CaCO_3$ gasifying agent were added to each chemical composition corresponding to 1 wt%, 2 wt% and 3 wt% of gas evolution during the reaction. Calcium nitride decomposes into calcium and nitrogen gas ($Ca_3N_2 \rightarrow 3Ca + N_2$) at 1195 °C while calcium carbonate decomposes into solid CaO and CO_2 gas ($CaCO_3 \rightarrow CaO + CO_2$) at 800 °C during the combustion synthesis reaction. The synthesis process and analysis of these composites was explained in detail elsewhere [11].

Archimedes principle was employed to determine apparent (open) porosity of the products [24]. A cylindrical sample was cut into wafers from the bottom of the sample to the top using a diamond blade saw. Each wafer was cut to measure approximately 1 mm wide allowing for extraction of eight wafers from each sample. The wafers were ground and polished using 600 grit SiC paper ensuring contrast between pores and the surrounding matrix. LECO IA32 imaging software [25] coupled with an optical microscope (Olympus PMG3 Metallograph, LECO Inc.) was used to resolve pore size and the relative distribution of pores on the surface of the wafers. A magnification of 5× was employed to separate each sample wafer into individual fields such that statistically accurate reporting of pore sizes and distribution was assured. Each field covered approximately 1.78 mm^2 of surface area and pores were measured using a consistent designation of 0.0021×0.0028 mm^2 pixels with a constant attenuation threshold of 35 out of 255. Photomicrographs of the porous sample surfaces were obtained using a FEI Quanta 600 environmental scanning electron microscope (ESEM).

Results and discussion

Apparent (open) porosity determined using Archimedes principle as a function of moles gasifying agent added to the chemical compositions is presented in Fig. 1. The sample size consisted of five measurements with data points representing average values while error bars represent standard deviations.

Both gasifying additives show increased final product porosity for the TiC-30 wt% Ni_3Ti. The increasing trend is almost linear for the additives as the molar amount was increased. The $CaCO_3$ gasifying agent exhibited a slightly greater increase in product porosity than did the Ca_3N_2 gasifying agent. Product porosity increased 25% with a $CaCO_3$ gasifying agent, ranging from 58% porosity with no additive to 77% porosity with 0.25 moles gasifying agent, and increased 15% with a Ca_3N_2 gasifying agent, ranging from 58% porosity with no additive to 68% porosity with 0.09 moles gasifying agent. Final product porosity employing these gasifying agents with the TiC-30 wt% Ni_3Ti exceed the ''target'' range for bone replacement materials, i.e. 40–60% porosity.

The $CaCO_3$ gasifying agent also exhibited a slightly larger increase in product porosity over the Ca_3N_2 gasifying agent for the TiC-50 wt% Ni_3Ti with a near linear relationship between porosity and amount of $CaCO_3$ incorporated into the SHS reaction. The porosity increased 38% with the $CaCO_3$ ranging from 40% porosity with no gasifying agent to 65% porosity with 0.16 moles gasifying agent. The apparent porosity values fall within the target range for bone replacement materials nicely. Addition of Ca_3N_2 to the reactant mixture increased product porosity only 19% ranging from 40% porosity with no gasifying agent to 50% porosity with 0.06 moles gasifying agent. However, these porosity values still fall within the target range.

The molar amount of gasifying agent added to the chemical composition significantly controlled final product porosity. An increase in the molar amount of gasifying agent corresponds to an increase in the moles of gas released during the reaction. In turn, the increase in moles of gas release increases the apparent porosity of the synthesized product. Less moles of

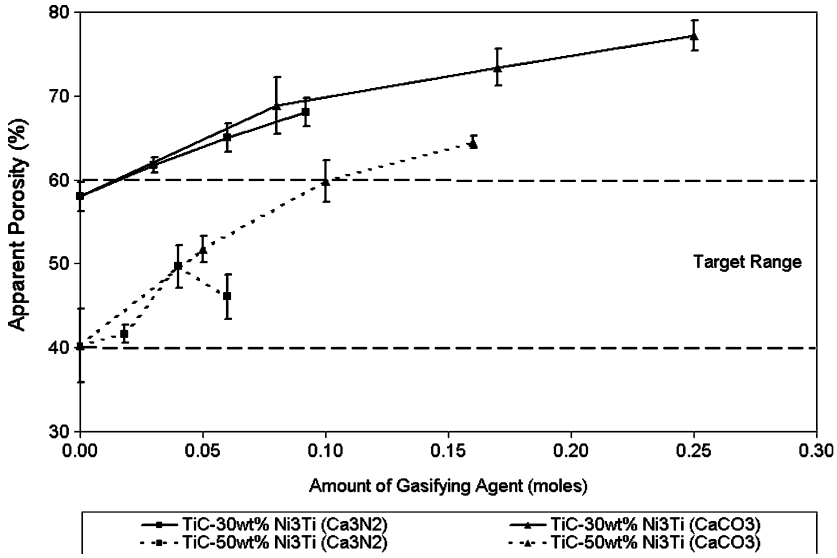

Fig. 1 Apparent (open) porosity as a function of moles gasifying agent added to the chemical compositions. The apparent porosity increased with increasing molar additions of gasifying agent

Ca_3N_2 gasifying agent than $CaCO_3$ gasifying were used for the investigation because weight percent of gas evolved was held constant, i.e. 1, 2 and 3 wt%. However, one mole of Ca_3N_2 yields three moles of Ca gas (and one mole of nitrogen that reacts with titanium) to only one mole of CO_2 gas produced from one mole of $CaCO_3$. Therefore, in effect, investigations involving the Ca_3N_2 gasifying agent result in lower molar amounts of gas release than those investigations involving the $CaCO_3$ gasifying agent. This corresponds to the higher observed apparent porosities for $CaCO_3$ than Ca_3N_2. It should be noted that increases in Ca_3N_2 gasifying agent beyond 3 wt% Ca gas evolved during the reaction resulted in extremely 'dirty' reactions, that make viewing propagation almost impossible, and greatly reduced the sample's structural integrity.

LECO image analysis for distribution of pores and corresponding pore sizes are presented in Figs. 2, 4, 6 and 8. Data are presented in an effort to show variation of pore size distribution as a function of cumulative frequency percent. Examination of Fig. 2 suggests that addition of Ca_3N_2 gasifying agent to the TiC-50 wt% Ni_3Ti gives rise to a variable distribution of pores on the order of 101–500 μm.

Cumulative frequency distribution of pores in the target range, i.e. 101–500 μm, exhibited the following trends with increasing moles of Ca_3N_2 gasifying agent: from 0.02 moles to 0.04 moles Ca_3N_2 gasifying agent the cumulative frequency percent of pores in the target range increased from 6.4% to 18%; from 0.04 moles to 0.06 moles Ca_3N_2 gasifying agent the frequency percent of pores in the target range decreased slightly from 18 to 11%. Hence, the optimal yield of pores in the designated target range of 101–500 μm was obtained when 0.04 moles Ca_3N_2 in the TiC-50 wt% Ni_3Ti SHS reaction was employed. However, both 0.02 mole and 0.06 mole Ca_3N_2 gasifying agent additions yield significant increases in target pore size range over a reaction with no gasifying agent addition (3.5%).

SEM photomicrographs of the surfaces of the TiC-50 wt% Ni_3Ti with Ca_3N_2 gasifying agent are provided in Fig. 3. Examination of the SEM photomicrographs revealed no significant increases in porosity formation. Large pores are formed in all three samples, but the 0.04 mole Ca_3N_2 sample produced the greatest distribution of large pores while the 0.02 mole Ca_3N_2 sample produced the smallest distribution of large pores.

A condition of slightly pulsating combustion phenomena could explain the observed distribution shifts in cumulative frequency percent of pores in the target range [26]. Kinetics of the evolution of a gaseous species, and subsequently coalescent phenomena that brings about the formation of larger pores (on the order of 101–500 μm), is dependent on the gas pressure generated inside the pores and the viscosity of the melt at the combustion front. Elongation of the sample, in turn, is dependent upon melt viscosity and burning velocity of the reaction front [27, 28]. Therefore, in the case of pulsating combustion, any perturbation in burning velocity could result in variations in sample elongations and indirectly to a variable viscosity in the melt at the reaction front, gas evolution reactions, and solidification rates that allow for growth of smaller pores into larger pores and pores that have increased interconnectivity.

The response of the 101–500 μm target pore size distribution was less sensitive to the selected gasifying

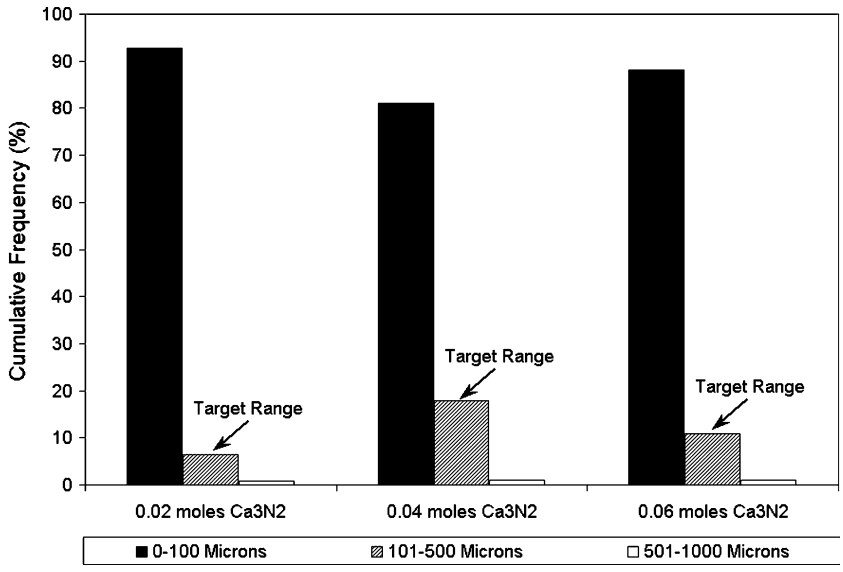

Fig. 2 Cumulative pore size frequency distribution as a function of moles Ca_3N_2 gasifying agent with the TiC-50 wt% Ni_3Ti. The greatest increase of pores within the target range occurred for TiC-50 wt% Ni_3Ti reacted with 0.04 moles Ca_3N_2

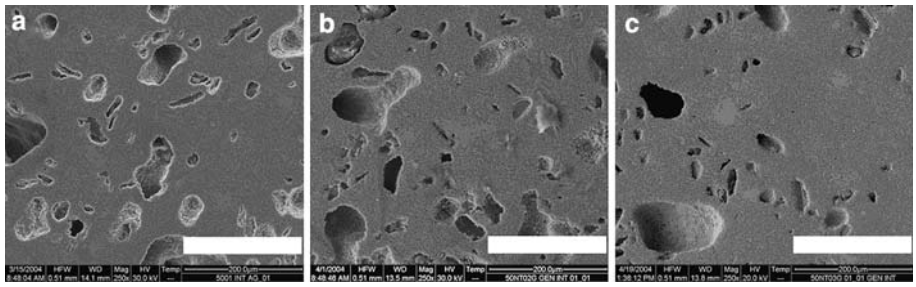

Fig. 3 SEM photomicrographs at 250× magnification of TiC-50 wt% Ni_3Ti with (**a**) 0.02 moles, (**b**) 0.04 moles and (**c**) 0.06 moles Ca_3N_2 gasifying agent. The scale bars represent 250 μm

agents for the remaining three SHS reaction systems. The same incremental increase or decrease in the target pore size range was not as significant as that observed for the TiC-50 wt% Ni_3Ti with increasing molar amounts of Ca_3N_2. The observed responses from Figs. 4, 6 and 8, respectively, were as follows.

The cumulative frequency distribution of pores within the target range steadily decreased with an increase in gasifying agent for the TiC-50 wt% Ni_3Ti with $CaCO_3$ (Fig. 4), although a constant increase in apparent porosity was observed. The steady decrease gave rise to a gradual increase in the distribution of pores that fell within the 0–100 μm size range. SEM photomicrographs of the TiC-50 wt% Ni_3Ti with $CaCO_3$ gasifying agent are presented in Fig. 5. Observation of Fig. 5 revealed that the apparent porosity of the samples increased with increasing molar amounts of $CaCO_3$ gasifying agent. In addition, the degree of interconnectivity among the pores increased with increasing molar amounts of $CaCO_3$ gasifying agent. Pore size and pore distribution are not greatly affected by the gasifying agent addition, confirming the trend observed in Fig. 4.

A modest effect in pore size was observed among TiC-30 wt% Ni_3Ti reacted with Ca_3N_2 gasifying agent (Fig. 6). SEM photomicrographs of the TiC-30 wt% Ni_3Ti with Ca_3N_2 gasifying agent are provided in Fig. 7. The decreasing trend in larger pore sizes and the degree of interconnectivity with increasing Ca_3N_2 observed in Fig. 7 is consistent with results presented in Fig. 6 for increasing molar amounts of Ca_3N_2. The increase in apparent porosity with increasing molar amounts of Ca_3N_2 gasifying agent is the result of increased small pore formation, i.e. 0–100 μm.

A slight increase in the distribution of pores within the target range was observed for increased $CaCO_3$ gasifying agent additions to the TiC-30 wt% Ni_3Ti reaction (Fig. 8). SEM photomicrographs of the TiC-30 wt% Ni_3Ti with $CaCO_3$ gasifying agent are provided in Fig. 9. The SEM photomicrographs revealed significant increases in product porosity and pore interconnectivity that compliments data from Fig. 1, and no increase in pore sizes falling within the 101–500 μm range with increasing molar amounts of $CaCO_3$ gasifying agent was observed. In general, all of these trends demonstrate a variety of observed effects the gasifying agents have on pore size distribution.

Reaction phenomena proposed earlier (instability oscillations during the SHS reaction) could be responsible for perturbing steady state combustion front

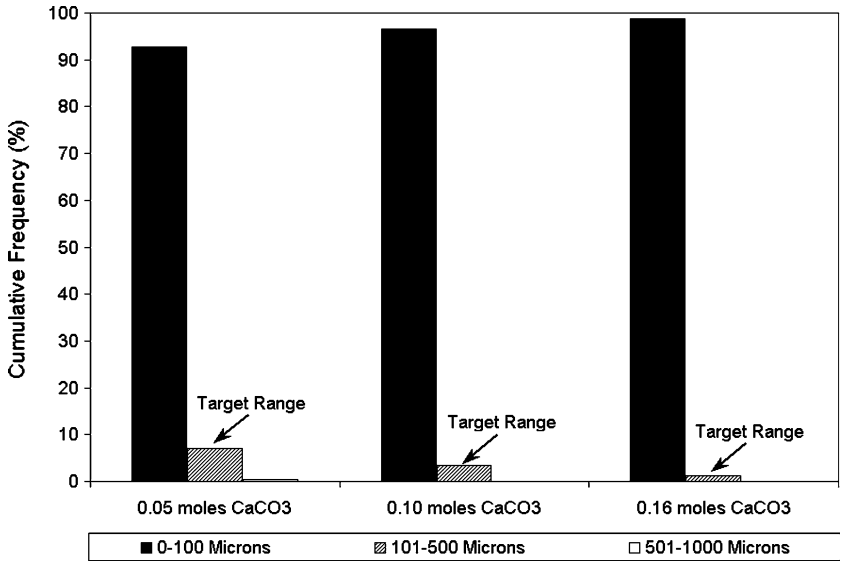

Fig. 4 Cumulative pore size frequency distribution as a function of moles $CaCO_3$ gasifying agent with the TiC-50 wt% Ni_3Ti. The greatest increase of pores within the target range occurred for TiC-50 wt% Ni_3Ti reacted with 0.05 moles $CaCO_3$

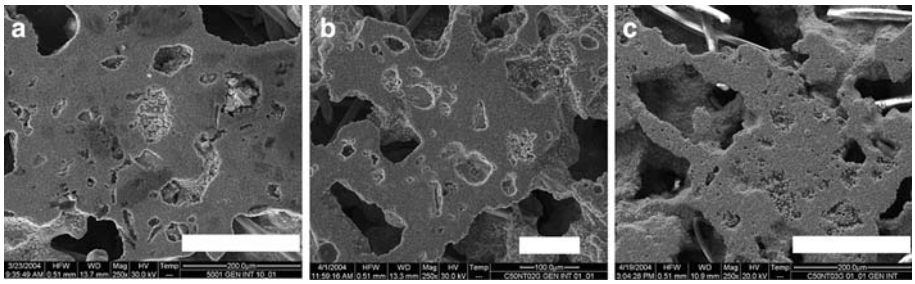

Fig. 5 SEM photomicrographs at 250× magnification of TiC-50 wt% Ni_3Ti with (**a**) 0.05 moles, (**b**) 0.10 moles and (**c**) 0.16 moles $CaCO_3$ gasifying agent. Scale bars in photomicrographs (**a**) and (**c**) represent 200 μm while the scale bar in photomicrograph (**b**) represents 100 μm

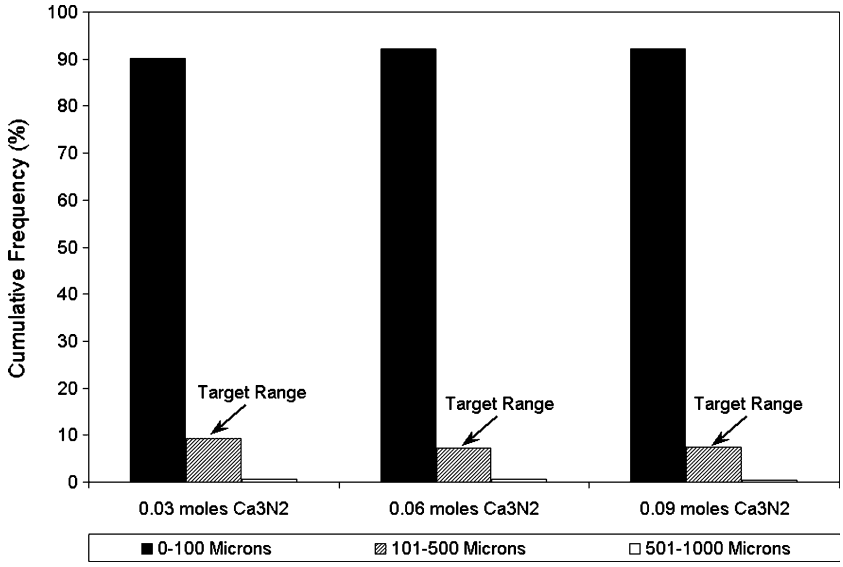

Fig. 6 Cumulative pore size frequency distribution as a function of moles Ca_3N_2 gasifying agent with the TiC-30 wt% Ni_3Ti. The greatest increase of pores within the target range occurred for TiC-30 wt% Ni_3Ti reacted with 0.03 moles Ca_3N_2

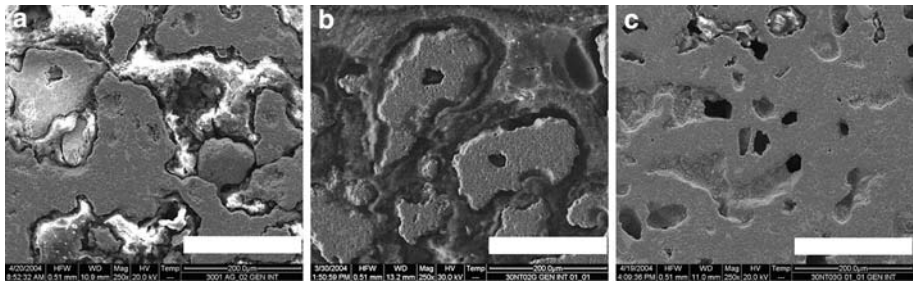

Fig. 7 SEM photomicrographs at 250× magnification of TiC-30 wt% Ni_3Ti with (**a**) 0.03 moles, (**b**) 0.06 moles and (**c**) 0.09 moles Ca_3N_2 gasifying agent. Scale bars in the photomicrographs represent 200 μm

propagation. These perturbations ultimately give rise to observed characteristics for the cumulative pore size distribution. For example, in order to establish conditions necessary to retard a combustion reaction and incite a pulsating combustion mode, reaction kinetics must experience variation in the rate of reaction. Evolution of calcium gas (from Ca_3N_2) could possibly incite such variation in that it could serve as a ''heat sink'', or diluent, when surrounded by the intermetallic melt, since it is a metal (i.e. high thermal conductivity). However, observed results for TiC-50 wt% Ni_3Ti with Ca_3N_2 gasifying agent do not support this hypothesis. If calcium gas is acting as a heat sink and effectively slowing the rate of reaction resulting in burning velocity perturbations, it is doing so in conjunction with additional effects unique to this reaction system, i.e. an increase in volume fraction of the intermetallic melt during the exothermic SHS reaction.

Combustion temperature, reaction pressure, burning velocity and percentage of linear expansion of the chemical compositions and gasifying agents is

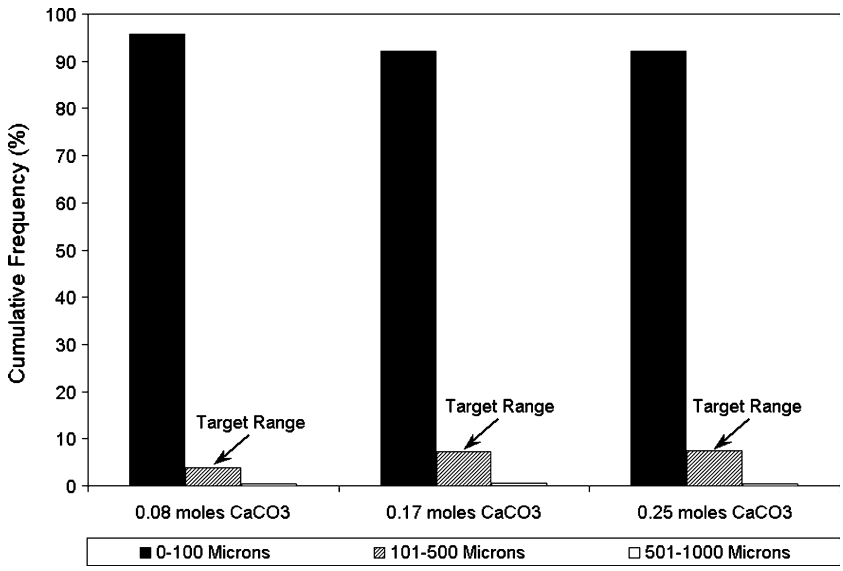

Fig. 8 Cumulative pore size frequency distribution as a function of moles $CaCO_3$ gasifying agent with the TiC-30 wt% Ni_3Ti. The greatest increase of pores within the target range occurred for TiC-30 wt% Ni_3Ti reacted with 0.17 moles $CaCO_3$

presented in Table 1 for the TiC-30 wt% Ni_3Ti and Table 2 for the TiC-50 wt% Ni_3Ti. The data presented in Tables 1 and 2 was obtained from the combustion synthesis experiments presented in Ref. [11].

Observation of the data presented in Table 1 revealed the following relationships for the TiC-30 wt% Ni_3Ti chemical composition with Ca_3N_2 gasifying agent: an increase in the moles of gasifying agent added to the chemical composition increased reaction pressure, burning velocity, percentage of linear elongation and decreased the cumulative frequency of pores present within the 101–500 μm target range (Fig. 6) and pore interconnectivity (Fig. 7). Increasing the moles of Ca_3N_2 gasifying agent to the chemical composition would ideally increase the reaction pressure since more gas is evolved from the gasifying agent. Burning velocity is increased as molar amounts of gasifying agent were increased resulting from the synthesis of reactant titanium with the decomposition product nitrogen from Ca_3N_2. In other words, although the Ca_3N_2 gasifying agent initially acts as a diluent during the combustion reaction requiring energy to decompose, some of the energy is recovered due to the highly exothermic titanium–nitrogen reaction, therefore increasing burning velocity. Increased reaction pressure leads to higher percentages of linear elongation, and in this case decreased pore interconnectivity. An increase in percentage of linear elongation should indicate increased pore interconnectivity as more surface area is exposed for the gas to escape at or ahead of the reaction front to the environment, therefore raising reaction pressure observed in the combustion chamber. However, this is not observed and results from the lower combustion temperature with the highest molar amount of Ca_3N_2 gasifying agent that increased viscosity of the melt present in the combustion wave, thereby decreasing pore interconnectivity. Furthermore, since the combustion wave is much faster for this case the gas pockets in the viscous combustion wave do not have much time to agglomerate forming larger pores, resulting in decreased cumulative frequency of pores within the target range.

Similarly, observation of data presented in Table 1 revealed the following relationships for the TiC-30 wt% Ni_3Ti chemical composition with $CaCO_3$ gasifying agent: an increase in the moles of gasifying agent added to the chemical composition increased reaction pressure, percentage of linear elongation, cumulative

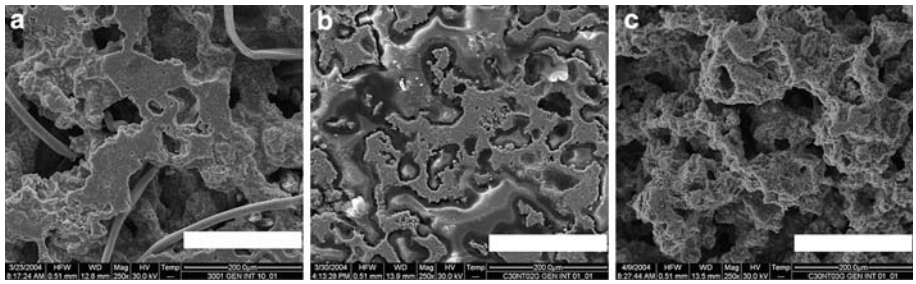

Fig. 9 SEM photomicrographs at 250× magnification of TiC-30 wt% Ni_3Ti with (**a**) 0.08 moles (**b**) 0.17 moles and (**c**) 0.25 moles $CaCO_3$ gasifying agent. Scale bars in the photomicrographs represent 200 μm

Table 1 Combustion temperature (T_c), reaction pressure (P), burning velocity (v) and percentage of linear elongation ($\Delta l/l$) for the TiC–30 wt% Ni_3Ti and gasifying agents [11]

Moles of gasifying agent	T_c (°C)	P (kPa)	v (mm sec^{-1})	$\left(\frac{\Delta l}{l}\right)$
0.03 Ca_3N_2	2272	153.6	8.02	11.6
0.06 Ca_3N_2	2347	153.6	7.01	15.7
0.09 Ca_3N_2	2266	154.5	9.42	18.1
0.08 $CaCO_3$	2289	134.8	6.26	11.1
0.17 $CaCO_3$	2360	142.9	5.27	22.9
0.25 $CaCO_3$	2245	149.4	4.67	23.2

Table 2 Combustion temperature (T_c), reaction pressure (P), burning velocity (v) and percentage of linear elongation ($\Delta l/l$) for the TiC-30 wt% Ni_3Ti and gasifying agents [11]

Moles of gasifying agent	T_c (°C)	P_1 (kPa)	v (mm sec^{-1})	$\left(\frac{\Delta l}{l}\right)$
0.02 Ca_3N_2	1784	135.3	2.40	2.7
0.04 Ca_3N_2	1901	101.9	2.42	1.2
0.06 Ca_3N_2	1942	119.1	4.46	7.9
0.05 $CaCO_3$	1753	65.8	1.82	-0.3
0.10 $CaCO_3$	2017	85.8	3.17	6.1
0.16 $CaCO_3$	2132	123.4	3.81	8.1

frequency of pores present within the 101–500 μm target range (Fig. 8), pore interconnectivity (Fig. 9) and decreased burning velocity. Reaction pressure and percentage of linear elongation relationships are the same as those presented for the TiC-30 wt% Ni_3Ti with Ca_3N_2. However, burning velocity decreased with increased molar amounts of $CaCO_3$ because this gasifying agent acts purely as a diluent removing energy from the combustion reaction, with no additional synthesis between the reactants and decomposition products. Similar to the Ca_3N_2 gasifying agent, the highest molar amount of $CaCO_3$ with TiC-30 wt% Ni_3Ti has the lowest combustion temperature that increased melt viscosity. However, since burning velocity is much slower for this case, the gas pockets have time to agglomerate together in the molten reaction front forming larger pores and resulting in increased cumulative frequency percent of pores within the target range. Pore interconnectivity increased because overall pore size was increased.

Observation of data presented in Table 2 revealed the following relationships for the TiC-50 wt% Ni_3Ti chemical composition with Ca_3N_2 gasifying agent: an increase in the moles of gasifying agent added to the chemical composition increased combustion temperature, burning velocity, percentage of linear elongation, decreased cumulative frequency of pores present within the 101–500 μm target range (Fig. 2) and pore interconnectivity (Fig. 3), and gave rise to variable reaction pressure. Reaction pressure and percentage of linear elongation relationships are the same as those presented for the TiC-30 wt% Ni_3Ti cases. The increase in combustion temperature and burning velocity are again the result of the highly exothermic titanium–nitrogen reaction resulting from decomposition of Ca_3N_2. Since burning velocity increased with increased molar amounts of gasifying agent gas pockets in the less viscous reaction front (higher combustion temperatures) do not have much time to agglomerate to form larger pores, resulting in decreased cumulative frequency of pores within the target range.

Finally, observation of data presented in Table 2 revealed the following relationships for the TiC-50 wt% Ni_3Ti chemical composition with $CaCO_3$ gasifying agent: an increase in the moles of gasifying agent added to the chemical composition increased combustion temperature, reaction pressure, burning velocity, percentage of linear elongation, pore interconnectivity (Fig. 5) and decreased cumulative frequency of pores present within the 101–500 μm target range (Fig. 4). Relationships for reaction pressure, percentage of linear elongation, cumulative frequencies of pores in the target range and pore interconnectivity is similar to those already presented. However, the TiC-50 wt% Ni_3Ti with $CaCO_3$ has a different trend for combustion temperature and burning velocity than the TiC-30 wt% Ni_3Ti with $CaCO_3$. These differences were attributed to the thermal properties of the chemical compositions and the decomposing CO_2 gas in Ref. [11]. In addition, since decomposition molar amounts are lower for the TiC-50 wt% Ni_3Ti than the TiC-30 wt% Ni_3Ti, less energy is removed from the system by the inert decomposition products that act as a diluent in the system.

Microstructural analysis of the final products was presented in Ref. [11], however it should be pointed

out as a side note that excess nickel was present in the final product of the TiC-30 wt% Ni_3Ti chemical composition and Ca_3N_2 gasifying agent. The excess nickel resulted from reaction of titanium with the nitrogen decomposition product. Conversely, CaO was observed in the final product for the TiC-50 wt% Ni_3Ti and $CaCO_3$, as expected since CaO is a decomposition product. Trace amounts of CaO were also observed for the TiC-50 wt% Ni_3Ti with Ca_3N_2 that suggests all of the calcium gas did not escape the sample and oxidized after exposure to air. This was not necessarily observed for the TiC-30 wt% Ni_3Ti with Ca_3N_2 suggesting that a majority, i.e. >95% (XRD), of the gas did escape the sample (higher apparent porosities). These notes support the analysis provided above.

Although examinations presented in this paper did not provide a significant increase to pore sizes falling within a 101–500 μm range, speculations can be drawn from these results as to how a specific increase within this range can be obtained. For example, the physicochemical properties of the gasifying agent have been shown to be extremely important. It is apparent that the amount of gas, viscosity of the melt and burning velocity of the reaction are extremely important to forming larger pores. For example, a gasifying agent that produces ''heavier'' gas thereby increasing reaction pressures might be ideal, although safety and elemental reactions must be considered. Furthermore, the timing for release of the gas has been shown to be important through results within this paper. A decomposition temperature that is closer to the combustion temperature of the reaction might produce larger pores, as more of the gaseous decomposition product would be entering the viscous reaction front. A diluent could be added to the reactant stoichiometry to further control both reaction front viscosity and combustion temperature to additionally aid in formation of larger pores.

Conclusions

Addition of Ca_3N_2 and $CaCO_3$ gasifying agents increased final product porosity with increasing molar amounts of gasifying agent for both chemical compositions investigated (TiC-30 wt% Ni_3Ti and TiC-50 wt% Ni_3Ti). Final product porosity produced with these additives represent the general target range of 40–60% porosity for bone replacement materials. Pore size frequency percent was not significantly increased in the range of 101–500 μm for the TiC-50 wt% Ni_3Ti with $CaCO_3$, TiC-30 wt% Ni_3Ti with Ca_3N_2 and TiC-30 wt% Ni_3Ti with $CaCO_3$. However, pore size frequency was significantly increased in the range of 101–500 μm for TiC-50 wt% Ni_3Ti with Ca_3N_2, giving rise to the conclusion that this chemistry represented the best observed conditions for yielding pores within the target pore size range. Reaction phenomena, and any possible correlation between reaction phenomena and a pulsating combustion mode, could contribute to the observed increase in pore size frequency in the range of 101–500 μm.

Acknowledgements The authors wish to thank the Space Products Development directorate of NASA and the Director of the Institute for Space Resources, formerly CCACS, Dr. Michael Duke, for support of this work.

References

1. Munir ZA, Anslemi-Tamburini U (1989) Mater Sci Report 3:227
2. Munir ZA (1993) J Mat Syn Proc 1(6):387
3. Rice RW, McDonough WJ (1985) J Am Ceram Soc 68(5):C122
4. German RM (1989) Particle packing characteristics. Metal Powder Industries Federation, New Jersey
5. Wakeman RJ (1975) Powder Technol 11:297
6. Kirdyashkin AI, Maksimov YuM, Merzhanov AG (1981) Fiz Goreniya i Vzryva (Engl Trans) 17(6):10
7. Shkiro VM, Borovinskaya IP (1976) Fiz Goreniya i Vzryva (Engl Trans) 12(6):945
8. Dunmead SD, Munir ZA, Holt JB, Kingman DD (1991) J Mat Sci 26:2410
9. Shcherbakov VA, Merzhanov AG (1998) Combust Sci Technol 136:253
10. Ponomarev MA, Sapronov YuA, Shteinberg AS (1996) Combust Expl Shock Waves 32(3):286
11. Burkes DE, Yi HC, Gottoli G, Moore JJ (2006) J Mat Sci 41:2009
12. Li BY, Rong L-J, Li Y-Y, Gjunter VE (2000) Acta Mater 48:3895–3904
13. Ayers RA, Bateman TA, Simske SJ (2000) in Shape memory implants. Springer Verlag, Berlin, p 73
14. Itin VI, Shevchenko NA, Korosteleva EN, Tukhfatullin AA, Mirgazizov MZ, Gjunter VE (1997) Tech Phys Lett 23(4):294
15. Bronzino JD (ed) (1995) The biomedical engineering handbook. CRC Press, Boca Raton, FL, p 682
16. Cameron HU (1994) in ''Bone implant interface. Mosby, St. Louis, p 145
17. Moore JJ, Schowengerdt FD, Ayers R, Zhang X, Castillo M (2001) in Sixth Inter. Microgravity Comb. Workshop NASA/CP-2001–210826 p 273
18. Hulbert SF, Young FA, Mathews RS, Klawitter JJ, Talbert CD, Stelling FH (1970) J Biomed Mater Res 4:433
19. van Eeden SP, Ripamonti U (1994) Plast Reconstr Surg 93:959
20. Kim HK, Jang JW, Lee CH (2004) J Mat Sci: Mat in Med 15:825
21. Buser D, Schenk RK, Steinemann S, Fiorellini JP, Fox CH, Stich H (1991) J Biomed Mater Res 25:889

22. Rich A, Harris AK (1981) J Cell Sci 50:1
23. Thomas K, Cook S (1985) J Biomed Res 19:875
24. ASTM Designation (1992) C 20–92 p 5
25. LECO Corporation, St. Joseph, MO 49085
26. Merzhanov AG, Sytschev AE (2004) ''ISMAN'', http://www.ism.ac.ru/handbook/_shs.htm#prc3, as in May 2004
27. Merzhanov AG (1990) in Combustion and plasma-synthesis of high temperature materials. VCH Publishers, New York
28. Shteinberg AS, Shcherbakov VA, Marynov VV, Mukhoyan MZ, Merzhanov AG (1991) Sov Phys Dokl (Engl Trans) 36(5):385–387